Sensors and Materials, Vol. 36, No. 9 (2024) 4077–4087
MYU Tokyo

S & M 3785

Fundamental Characteristics of Molecularly Imprinted Polymer Nanoparticles with High Affinity for Human Serum Albumin

Youyuan Man, Shoichi Nishitani, and Toshiya Sakata*

Department of Materials Engineering, School of Engineering, The University of Tokyo,
7-3-1 Hongo, Bunkyo-ku, Tokyo 113-8656, Japan

(Received October 30, 2023; accepted April 15, 2024)

Keywords: Molecularly imprinted polymer nanoparticles, human serum albumin, solid-phase imprinting

In this research, the meticulous development and exhaustive analysis of molecularly imprinted polymer nanoparticles (nano-MIPs) are explored, with particular emphasis on their affinity for human serum albumin (HSA), a crucial biomarker for diagnosing type 2 diabetes mellitus. The yield of the synthesized nano-MIPs for HSA was determined by a freeze drying technique to be in the range of 6–15 mg for every 100 g of glass beads. A multifaceted characterization approach, including dynamic light scattering analysis, atomic force microscopy, and Fourier-transform infrared spectroscopy, was employed to rigorously assess the physicochemical properties of the nano-MIPs. The results indicate a relatively uniform size distribution and a well-defined chemical composition. Surface plasmon resonance kinetic analysis further revealed that the nano-MIPs exhibit high affinity and specificity for HSA, with a dissociation constant (Kd) of 2.37×10^{-9} M and an R^2 value of 0.97. These findings not only validate the successful synthesis and characterization of nano-MIPs but also underscore their potential use for selective molecular recognition, thereby providing promising avenues for future research and applications in biomedical and environmental fields.

1. Introduction

Human serum albumin (HSA), the most abundant protein in human blood plasma, is a key player in the body's functionality.[1–5] It carries out multiple essential tasks including maintaining the osmotic pressure in the blood and serving as a transporter of various substances within the body.[6,7] However, the importance of HSA extends beyond its physiological role – it also serves as a vital biomarker in diagnostic medicine.[8] For instance, the variation in HSA level can reflect the onset or progression of diabetes, thus making its detection a crucial component in blood glucose monitoring and management.[9,10]

Historically, immunochemical methods have been utilized to quantitatively measure albumin concentrations in serum and urine.[11,12] Although these methods have been technologically improved to increase their simplicity and accuracy,[13] they have limitations that cannot be

*Corresponding author: e-mail: sakata@biofet.t.u-tokyo.ac.jp
https://doi.org/10.18494/SAM4738

ISSN 0914-4935

overlooked, such as time-consuming procedures and high equipment costs. These have led to the exploration of alternative approaches for routine analysis.

As an alternative, the use of biosensors has been explored. Biosensors have demonstrated superior performance in the detection of various compounds and, as a result, have become the focal point of extensive global research.[14–17] Among various detection methods, the electrochemical method has gained widespread acceptance owing to its simplicity and quantification capability.[18–20] In this method, the electrical signals generated by the ions or electrons produced from the chemical reactions between a biorecognition element and the target analyte are measured. However, the effectiveness of this method depends on having a specific material to form a functionalized surface.

To functionalize surfaces, one promising solution that has emerged is the use of molecularly imprinted polymers (MIPs) owing to their low cost and robustness against natural materials such as enzymes.[21–27] These synthetic materials are designed to be highly selective towards a specific molecule. The process begins with the selection of target molecules as a template, followed by the formation of a complex with functional monomers through noncovalent interactions, such as hydrogen bonding or electrostatic interactions. A polymerization reaction then occurs, resulting in the creation of a rigid matrix around the template molecule, which is subsequently removed, often by washing with a suitable solvent. The result is a polymer matrix with cavities that perfectly match the template in size, shape, and functional group positioning.

However, the conventional MIP synthesis method described above poses some challenges.[28] One of the primary limitations is the production of heterogeneous polymers. This can result in an array of binding site conformations within the polymer, some of which may not interact efficiently with the target molecule. This heterogeneity subsequently diminishes the abundance of high-affinity binding sites that are essential for the selective identification of the target molecule. Another challenge with the conventional MIP synthesis method is the potential for residual template molecules to remain in the polymer matrix. Despite rigorous washing procedures after polymerization to remove template molecules, some may remain trapped within the matrix. These residual molecules can interfere with biomolecular recognition by occupying the binding sites meant for the target molecule. Consequently, the sensitivity and specificity of MIPs produced through these conventional methods can be compromised.

To overcome the challenges associated with the conventional MIP synthesis method, the solid-phase synthesis method has recently been developed.[29] In this method, MIP nanoparticles (nano-MIPs) with increased specificity and reduced heterogeneity are formed by utilizing the temperature-responsive properties of poly-N-isopropylacrylamide (NIPAAm),[30] wherein polymerization occurs on a template-coated solid phase below the lower critical solution temperature (LCST) of poly-NIPAAm to retain the template, and heating above the LCST thereafter ensures the efficient template release. Several instances of successful syntheses exemplify the adaptability and versatility of the method across a range of proteins or epitopes with specific peptide sequences and various characteristics and functions.[31–33] Proteins or epitopes, despite their diverse structures and functions, are fundamentally polymers of amino acids, sharing similar inherent biochemical properties and interaction potentials due to the universal presence of amino acid residues. These foundational biochemical similarities among

them imply a level of uniformity in their interactions with comonomers, providing a rational basis for the generalizability of the synthesis method across different proteins such as HSA.

In this study, we focus on the synthesis and characterization of nano-MIPs with a strong binding affinity for HSA. We aim to form nano-MIPs with increased specificity and reduced heterogeneity as the specific material for surface functionalization in electrochemical biosensors. Using various characterization techniques, we evaluate the binding affinity of these nano-MIPs for HSA in this study. The overarching goal is to improve diabetes diagnosis and management by providing a reliable, efficient, and cost-effective surface material for HSA detection.

2. Materials and Methods

2.1 Chemicals

Sulfuric acid (H_2SO_4), sodium hydroxide (NaOH), acetone, aminopropyltrimethoxysilane (APTMS), toluene anhydrous, HSA, sodium tetrahydroborate ($NaBH_4$), ethanolamine, NIPAAm, *N*,*N*'-methylenebisacrylamide (BIS), N-tert-butylacrylamide (TBAm), ethanol, acrylamide (AAm), *N*,*N*,*N*',*N*'-tetramethylethylenediamine (TEMED) ammonium peroxodisdulfate (APS), and cysteamine hydrochloride were purchased from Wako Pure Chemicals Industries, Ltd. Phosphate-buffered saline (PBS 1X, pH 7.4) was purchased from Thermo Fisher Scientific Inc. Glutaraldehyde was purchased from Tokyo Chemical Industry Co., Ltd. Spherical glass beads with diameters ranging from 63 to 88 μm (SGMT No. 007) were purchased from Toshinriko Co., Ltd. Glycated albumin (GA), which was purified from human serum, was supplied by PROVIGATE Inc., or a standard GA was purchased from the Reference Material Institute for Clinical Chemistry Standards (ReCCS, Japan).

2.2 Preparation of solid phase

Nano-MIPs were synthesized manually using cleaned and lab-grade glassware. Figure 1 outlines the process for solid phase preparation.[29] HSA was immobilized onto the silanized glass beads prior to nano-MIP synthesis. Briefly, glass beads (200 g) were activated by boiling in NaOH (4 M) for 30 min and washed thoroughly with Milli-Q water. Subsequently, the glass beads were incubated in 20% (v/v) sulfuric acid solution for 60 min. The beads were then washed sequentially with PBS, Milli-Q water, and acetone in this sequence, dried in an oven at 120 °C for 30 min, and silanized with 2% v/v APTMS in anhydrous toluene (100 mL) at 60 ºC overnight with stirring (170 rpm). Finally, the silanized glass beads were washed thoroughly with acetone and reconditioned by drying in the oven at 120 °C for 30 min. The resultant amine-functionalized glass beads were incubated with a 100 mL solution of glutaraldehyde in PBS (7% v/v, pH 7.4) at room temperature for 2 h. Subsequently, the glass beads were rinsed with milli-Q water and dried in a vacuum. The glass beads were then incubated at room temperature overnight with the template solution, which was prepared by dissolving HSA (1 mg/mL) in PBS (100 mL) with stirring (170 rpm). The beads were then rinsed with Milli-Q water and dried

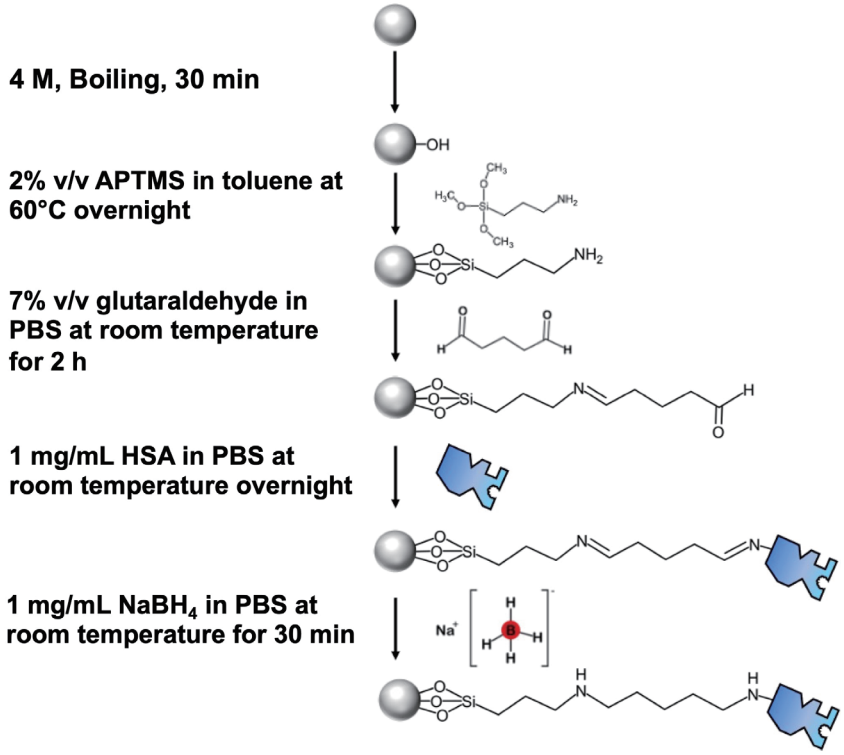

Fig. 1. (Color online) Schematic of immobilization of HSA template onto glass beads as solid phase.

completely in a vacuum. The remaining unreacted aldehyde groups were blocked with 100 mL of ethanolamine (0.01 M, pH 7.4). Schiff base bonds were reduced with 100 mL of $NaBH_4$ (1 mg/ml, pH 7.4) at room temperature for 30 min.

2.3 Synthesis of nano-MIPs

Figure 2 outlines the process for nano-MIP preparation, adapted from the methodology presented by Canfarotta *et al.*[29] Glass beads, derivatized and chemically immobilized with HSA, served as the solid phase, although the immobilization density of HSA on the beads was not estimated in this study. The polymerization mixture consisted of NIPAAm (29.4, 294, 588 mg), TBAm (24.8, 248, 496 mg), AAm (13.8, 138, 276 mg), and BIS (20, 40, 80 mg), all dissolved in 100 mL of water, where the sums of each concentration were adjusted to be 6.5, 65, and 130 mM. The derivatized glass beads (100 g) were added to this mixture, sonicated for 5 min, and subjected to N2 gas bubbling for 30 min. Polymerization was initiated by adding APS (27 mg) and TEMED (15 μL), and allowed to proceed at room temperature for 2 h. Subsequently, the modified beads were rinsed with distilled water at room temperature using a fritted solid-phase extraction (SPE) cartridge to eliminate low-affinity and unreacted components. High-affinity nano-MIPs for HSA were then collected by flushing the SPE cartridge with 100 mL of water at 60 °C. The solubility of nano-MIPs did not meet the requirements for employing the measurement technique at 60 °C. This means that the number of hydrophobic nano-MIPs composed of poly-NIPAAm increased at 60 °C, which should have exceeded the LCST of the nano-MIPs. For comparison, non-imprinted polymer nanoparticles (nano-NIPs) were produced

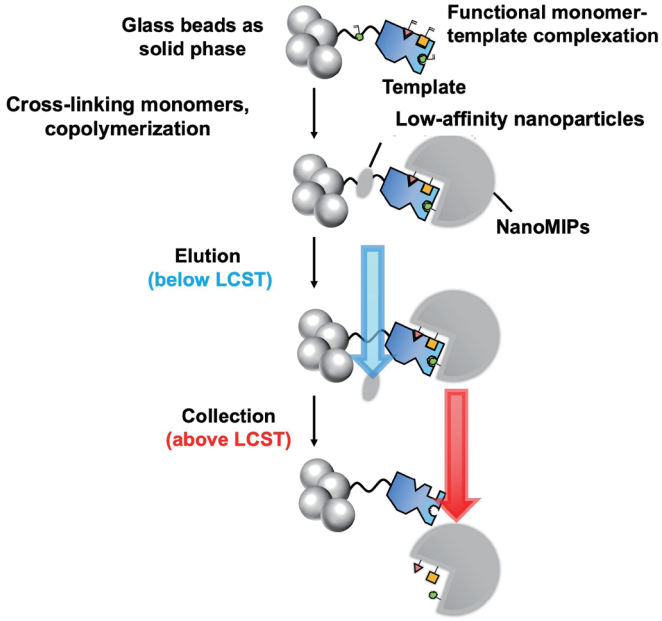

Fig. 2. (Color online) Synthesis of nano-MIPs.

by the same method, but without incorporating GA or HSA. 20 mL of the nano-MIP suspension was freeze-dried in a 50 mL Falcon tube. The resulting solid residue was then weighed to determine the concentration of the suspension.

2.4 Fourier-transform infrared spectroscopy (FTIR) analysis

The chemical structure of nano-MIPs was investigated using the JASCO FT/IR-6300FV spectroscopy system. To prepare the nano-MIP suspension samples, 1 mg of nano-MIP powder was suspended in 20 µL of water. The prepared samples were directly placed onto a ZnSe crystal, integrated into a single-reflection ATR device. Once dried, measurements were carried out at a constant temperature of 25 °C. The spectra were captured in the range of 4000–600 cm^{-1}, maintaining a resolution of 4 cm^{-1}.

2.5 Dynamic light scattering (DLS) measurements

The hydrodynamic diameter and size distribution of nano-MIPs were determined by DLS measurements, using an S-nanosizer from Malvern Ltd. (Malvern, UK). For the analysis, nano-MIPs were dissolved in PBS (pH 7.4) at a standard concentration of 1 mg/mL. The resulting solution was then sonicated at room temperature for 30 min and subsequently filtered through a 0.45 µm syringe filter. A 50 µL aliquot from this solution was transferred to a quartz cuvette for measurement. The particle-containing solution was exposed to light with a wavelength (λ) of 632.8 nm. All analyses were carried out at a constant temperature of 25 °C.

2.6 Atomic force microscopy (AFM) measurements

AFM measurements of nano-MIPs were conducted using a Veeco Metrology System (Model No. 920-006-101, Veeco Metrology, Santa Barbara, CA, USA). Air measurements were conducted in the tapping mode utilizing RTESP-300 probes from Bruker, CA, USA. These probes feature a cantilever length of 125 μm and a spring constant of 40 N/m. Scanning was set to cover an area of 2 × 2 μm^2 or 5 × 5 μm^2 at a rate of 2 μm/s. For the analysis, nano-MIPs were dissolved in water at a concentration of 50 μg/mL. A 20 μL sample of this solution was drop-cast onto gold-coated substrates. The prepared samples were then allowed to dry naturally under ambient room conditions overnight.

2.7 Surface plasmon resonance (SPR) sensor chip preparation and protein binding assessment

Silicon substrates were sectioned into approximately 1 × 1.8 cm^2 pieces and subsequently cleaned using acetone and methanol. Chromium and gold layers were deposited on these substrates using a sputtering system (ULVAC, Inc.). The prepared chips were then immersed in an ethanol solution containing 5 mM cysteamine and left at room temperature for 24 h. The sensor chips were then treated with 5 mM glutaraldehyde for 1.5 h. Afterward, 0.1 mg/mL nano-MIPs were prepared in a pH 6 phosphate buffer and introduced to the substrates, with which they were allowed to interact for 24 h.[34] The binding interactions between the HSA–nano-MIPs and the SPR sensor chips, which had immobilized nano-MIPs, were assessed at 25 °C. Protein solutions of various concentrations (0, 12.5, 25.0, 50.0, and 100.0 ng/mL) prepared in 5 mM PBS (pH 7.4) were continuously introduced to the sensor surface at a flow rate of 20 μL/min, each for a duration of 20 min. Following each introduction, any unbound molecules were thoroughly rinsed off by a 4 min injection of 5 mM PBS. Nano-NIPs were analyzed using the same method for comparison.

3. Results and Discussion

Regarding cost-effectiveness and simplicity in the synthesis process, only three monomers were selected: NIPAAm, TBAm, and AAm. TBAm contributes to the hydrophobicity of nano-MIPs, aiding in maintaining their structure in aqueous solutions. The composition of the monomers was determined to ensure sufficient solubility in aqueous solutions while maintaining a level of structural rigidity, which is crucial for their practical application. Nano-MIPs were synthesized in water, targeting a pH of around 5.2. This pH is close to the isoelectric point of HSA (4.2) and is favorable for the interaction of HSA with AAm, at which the number of binding sites for AAm on HSA increases to more than 100.[35] Moreover, HSA displays various conformations depending on pH.[36] It is possible that at pH 5.2, HSA has a conformation that exposes more binding sites or makes the existing sites more accessible to AAm, leading to an increased number of binding sites. On the other hand, an increased number of binding sites at pH

5.2 increase the specificity of the interaction between AAm and HSA. Additionally, AAm reacts with the thiol groups of HSA, indicating a targeted interaction between the two.[37] Although there are concerns about the weak binding nature of AAm to HSA, the specificity of the interaction might be advantageous in synthesizing nano-MIPs with distinct recognition sites for HSA.

In the initial trials, a concentration of 6.5 mM yielded only trace amounts of nano-MIPs that were undetectable with a microbalance after freeze drying. To improve the yield, the concentration was increased tenfold to 65 mM, resulting in an approximate yield in the range of 6–15 mg across multiple batches, which means the reliable yield for the evaluation of the nano-MIPs polymerized in this experiment. Furthermore, a twofold increase to 130 mM did not result in a proportional increase in yield, indicating a potential presence of a saturation point of the HSA imprinting. Given the solubility constraints and the excessive consumption of the monomers at elevated concentrations, 65 mM was identified as the optimal concentration for nano-MIP synthesis. However, the binding sites between HSA and the polymerized matrix may not have been easily dissociated owing to the multipoint binding, which may have resulted in the relatively low yield of nano-MIPs obtained in this study.

The size of nano-MIPs was characterized using both the DLS and AFM techniques. DLS analysis [Fig. 3(a)] revealed a mean hydrodynamic diameter of 245 nm with a polydispersity index (PDI) of 0.30. PDI represents the variation in sizes of nanoparticles in a sample, the value of which ranges from 0 to 1. A PDI close to 0 indicates that the nanoparticles in the sample are very uniform in size, meaning that the sample is nearly monodisperse. On the other hand, a PDI close to 1 indicates a broader distribution, that is, the nanoparticles vary significantly in size.[38] In this context, the PDI of 0.30 indicates a relatively uniform size distribution, which is often desirable in nanoparticle synthesis. On the other hand, AFM imaging provided a morphological representation of nano-MIPs, showing a diameter of approximately 100 nm [Fig. 3(b)]. The height distribution analysis from the AFM data obtained revealed an average depth of 100 ± 6 nm, closely in agreement with the observed diameter range [Fig. 3(c)], although the height distribution may not have correctly represented the statistical distribution owing to the limited number of nano-MIPs within this area. However, it is noteworthy that there is a discrepancy between the DLS and AFM measurements. This difference can be attributed to the drying effect inherent to AFM, potentially causing particle shrinkage or aggregation.

FTIR spectroscopy was employed to analyze the chemical bonding states and functional groups present in the nano-MIPs [Fig. 3(d)]. The acquired spectra exhibited a distinct peak at 3447 cm^{-1}, characteristic of N–H stretching in primary amide groups. Additional peaks at 2939 and 1684 cm^{-1} were observed, corresponding to C–H and C=O stretching, respectively. Furthermore, the peak at 1122 cm^{-1} indicates the presence of the $–C(CH_3)_3$ group.[39] These spectral features collectively contribute to a comprehensive understanding of the chemical composition of nano-MIPs.

To assess the nano-MIP affinity towards HSA, SPR was employed for real-time, label-free kinetic analysis. The use of SPR for real-time analysis is particularly noteworthy as it provides a dynamic view of binding interactions, which is crucial for applications requiring rapid detection and high specificity. GA was used as a relevant control in this study, given its substantial clinical

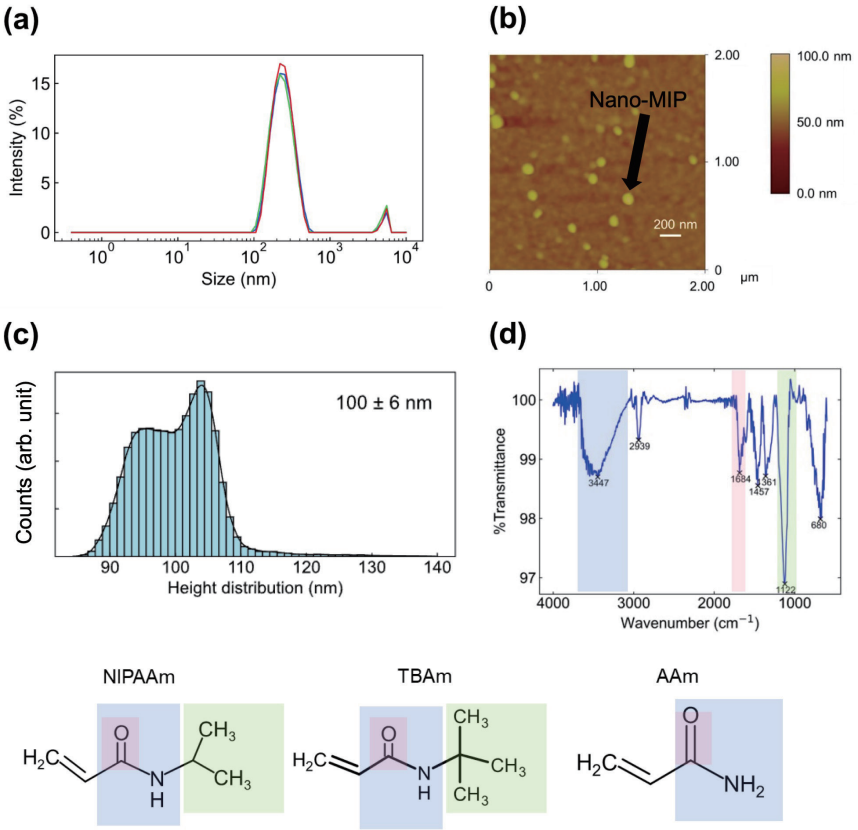

Fig. 3. (Color online) (a) DLS analysis of hydrodynamic size distribution of HSA–nano-MIPs. (b) AFM image of HSA–nano-MIPs (2 × 2 μm^2). (c) Height distribution of HSA-nano-MIP-deposited gold-coated substrate. A height distribution was extracted from a surface area of 5 × 5 μm^2. (d) FTIR spectra of HSA–nano-MIPs with chemical structures of the constituent monomers shaded to highlight the specific functional groups.

significance, particularly in the context of diabetes. GA is a modified form of HSA, resulting from the nonenzymatic glycation of the albumin protein.[9] It serves as a crucial clinical biomarker and an indicator of long-term glycemic control, allowing for a more accurate assessment and management of patients with diabetes.[40] The ability to distinguish between HSA and GA is therefore of importance in clinical diagnostics, enhancing the precision in evaluating glycemic status. Considering its structural similarities with HSA, GA serves as a control to assess the specificity of the nano-MIPs. As shown in Fig. 4(a), the sensorgram for nano-MIPs indicated a significant increase in SPR response level with HSA concentration, thereby confirming binding activity. The nano-MIP–HSA sensorgram demonstrated the spike signals upon adding HSA, indicating the interactions between HSA and the SPR sensor chip. After washing the SPR sensor chip with PBS, that is, the bound/free (B/F) molecule separation, the SPR responses clearly decreased while the response levels were maintained to a certain degree owing to the nano-MIP–HSA binding. In contrast, the sensorgram for nano-NIPs exhibited a lower SPR response level, underscoring the superior selectivity of nano-MIPs over nano-NIPs. The binding affinity of nano-MIPs to HSA was quantified by fitting the increasing

SPR levels against concentrations using a Langmuir isotherm model, thereby obtaining a dissociation constant (Kd) of 2.37×10^{-9} M and an R^2 value of 0.97 [Fig. 4(b)]. According to the SPR data, the fitted Langmuir isotherm is assumed to be typical and sigmoidal, which implies a 1:1 stoichiometry between the nano-MIPs and HSA. This suggests that the binding sites within the nano-MIPs exhibited a narrow distribution, indicative of uniform binding interactions. Furthermore, the SPR response level for HSA was markedly higher than that for GA, highlighting the capability of nano-MIPs to differentiate between HSA and its structurally similar counterpart, GA (Fig. 5). The low Kd and high R^2 values not only support the high affinity and specificity of nano-MIPs for HSA but also suggest potential applications of nano-MIPs in highly sensitive diagnostic assays in which distinguishing between HSA and GA is crucial.

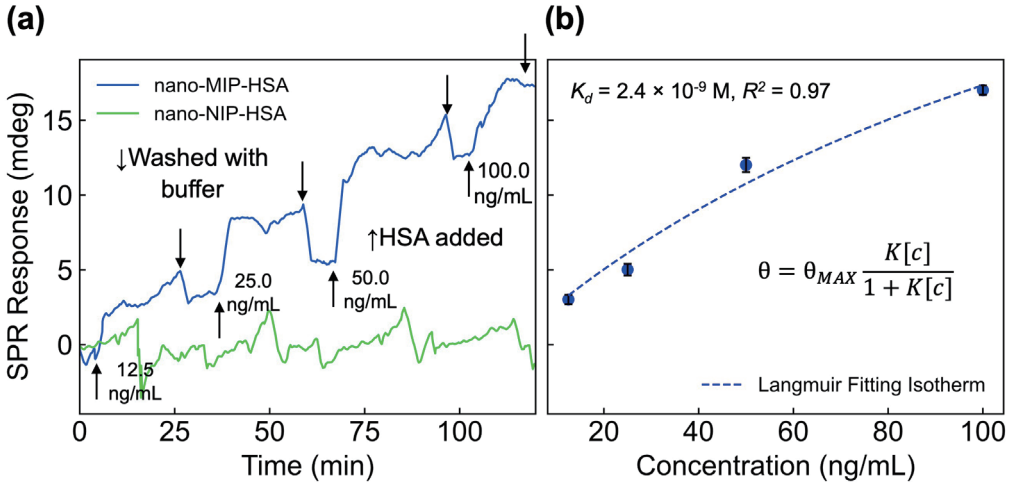

Fig. 4. (Color online) (a) SPR sensorgram showing HSA–nano-MIP/NIP binding interactions. (b) Concentration-dependent HSA binding represented through Langmuir isotherm fitting.

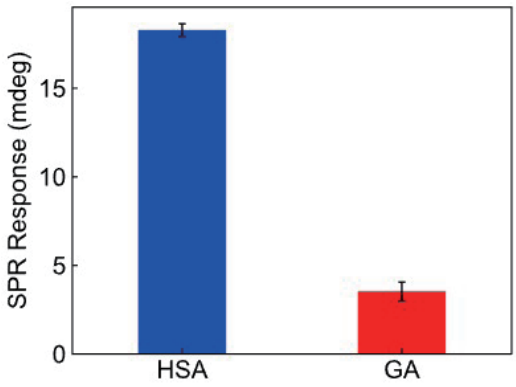

Fig. 5. (Color online) Differential SPR signals for HSA and GA for examining cross-reactivity at set concentration of 100 ng/mL.

4. Conclusion

This study provides a comprehensive evaluation of the synthesis and characterization of nano-MIPs, underscoring their potential utility in selective molecular recognition applications. Through a meticulous freeze drying process, the yield of the nano-MIPs was quantified to be in the range of 6–15 mg per 100 g of glass beads. A series of characterization techniques, including DLS, AFM, and FTIR spectroscopy, were employed to rigorously assess the physicochemical properties of the synthesized nano-MIPs. The data collectively indicate a relatively uniform size distribution and a well-defined chemical composition, which are the attributes highly desirable for targeted molecular interactions. Furthermore, SPR kinetic analysis revealed the high affinity and specificity of the nano-MIPs for HSA, as evidenced by a Kd value of 2.37×10^{-9} M and an R^2 value of 0.97. These findings not only validate the successful synthesis of nano-MIPs but also highlight their potential for selective molecular recognition, thereby opening avenues for further research and potential applications in biomedical and environmental fields.

References

1 K. Langer, S. Balthasar, V. Vogel, N. Dinauer, H. Von Briesen, and D. Schubert: Int. J. Pharm. **257** (2003) 169. https://doi.org/10.1016/S0378-5173(03)00134-0
2 G. Fanali, A. Di Masi, V. Trezza, M. Marino, M. Fasano, and P. Ascenzi: Mol. Aspects Med. **33** (2012) 209. https://doi.org/10.1016/j.mam.2011.12.002
3 R. Pieper, Q. Su, C. L. Gatlin, S.-T. Huang, N. L. Anderson, and S. Steiner: Proteomics **3** (2003) 422. https://doi.org/10.1002/pmic.200390057
4 G. D. J. B. Sudlow, D. J. Birkett, and D. N. Wade: Mol. Pharmacol. **11** (1975) 824.
5 D. C. Carter and X.-M. He: Science **249** (1990) 302. https://doi.org/10.1126/science.2374930
6 V. L. Vilker, C. K. Colton, and K. A. Smith: J. Colloid Interface Sci. **79** (1981) 548. https://doi.org/10.1016/0021-9797(81)90106-5
7 A. Wunder, U. Muller-Ladner, E. Stelzer, E. Neumann, H. Sinn, S. Gay, and C. Fiehn: Arthritis Res. Ther. **5** (2003) 1. https://doi.org/10.1186/ar810
8 M. E. Sitar, S. Aydin, and U. Cakatay: Clin. Lab. **59** (2013) 945. https://doi.org/10.7754/Clin.Lab.2012.121115
9 J. Anguizola, R. Matsuda, O. S. Barnaby, K. S. Hoy, C. Wa, E. DeBolt, M. Koke, and D. S. Hage: Clin. Chim. Acta **425** (2013) 64. https://doi.org/10.1016/j.cca.2013.07.013
10 A. Guérin-Dubourg, A. Catan, E. Bourdon, and P. Rondeau: Diabetes Metab. **38** (2012) 171. https://doi.org/10.1016/j.diabet.2011.11.002
11 S. Choi, E. Y. Choi, D. J. Kim, J. H. Kim, T. S. Kim, and S. W. Oh: Clin. Chim. Acta **339** (2004) 147. https://doi.org/10.1016/j.cccn.2003.10.002
12 K. Spencer and C. P. Price: Clin. Chim. Acta **95** (1979) 263. https://doi.org/10.1016/0009-8981(79)90368-1
13 J.-F. Xu, Y.-S. Yang, A.-Q. Jiang, and H.-L. Zhu: Crit. Rev. Anal. Chem. **52** (2022) 72. https://doi.org/10.1080/10408347.2020.1789835
14 S. P. Mohanty and E. Kougianos: IEEE Potentials **25** (2006) 35. https://doi.org/10.1109/MP.2006.1649009
15 P. Mehrotra: J. Oral Biol. Craniofac. Res. **6** (2016) 153. https://doi.org/10.1016/j.jobcr.2015.12.002
16 P. T. Kissinger: Biosens. Bioelectron. **20** (2005) 2512. https://doi.org/10.1016/j.bios.2004.10.004
17 V. Naresh and N. Lee: Sensors **21** (2021) 1109. https://doi.org/10.3390/s21041109
18 N. J. Ronkainen, H. B. Halsall, and W. R. Heineman: Chem. Soc. Rev. **39** (2010) 1747. https://doi.org/10.1039/b714449k
19 J. L. Hammond, N. Formisano, P. Estrela, S. Carrara, and J. Tkac: Essays Biochem. **60** (2016) 69. https://doi.org/10.1042/EBC20150008
20 D. Grieshaber, R. MacKenzie, J. Vörös, and E. Reimhult: Sensors **8** (2008) 1400. https://doi.org/10.3390/s8031400
21 J. J. BelBruno: Chem. Rev. **119** (2019) 94. https://doi.org/10.1021/acs.chemrev.8b00171
22 E. Turiel and A. Martín-Esteban: Anal. Chim. Acta **668** (2010) 87. https://doi.org/10.1016/j.aca.2010.04.019
23 K. Haupt, A. V. Linares, M. Bompart, and B. T. S. Bui: Molecular Imprinting (Springer, Heidelberg, 2012) p. 1.

24 R. Schirhagl: Anal. Chem. **86** (2014) 250. https://doi.org/10.1021/ac401251j
25 G. Vasapollo, R. Del Sole, L. Mergola, M. R. Lazzoi, A. Scardino, S. Scorrano, and G. Mele: Int. J. Mol. Sci. **12** (2011) 5908. https://doi.org/10.3390/ijms12095908
26 T. Kajisa and T. Sakata: ACS Appl. Mater. Interfaces **10** (2018) 34983. https://doi.org/10.1021/acsami.8b13317
27 T. Sakata, S. Nishitani, and T. Kajisa: RSC Adv. **10** (2020) 16999. https://doi.org/10.1039/D0RA02793F
28 S. C. Zimmerman and N. G. Lemcoff: Chem. Commun. (2004) 5. https://doi.org/10.1039/B304720B
29 F. Canfarotta, A. Poma, A. Guerreiro, and S. Piletsky: Nat. Protoc. **11** (2016) 443. https://doi.org/10.1038/nprot.2016.030
30 D. Schmaljohann: Adv. Drug Deliv. Rev. **58** (2006) 1655. https://doi.org/10.1016/j.addr.2006.09.020
31 M. Chiarello, L. Anfossi, S. Cavalera, F. Di Nardo, T. Serra, F. Sordello, and C. Baggiani: J. Mater. Chem. B **10** (2022) 6724. https://doi.org/10.1039/D2TB00245K
32 S. A. Piletsky, T. S. Bedwell, R. Paoletti, K. Karim, F. Canfarotta, R. Norman, D. J. L. Jones, N. W. Turner, and E. V. Piletska: J. Mater. Chem. B **10** (2022) 6732. https://doi.org/10.1039/D2TB00278G
33 F. Canfarotta, L. Lezina, A. Guerreiro, J. Czulak, A. Petukhov, A. Daks, K. Smolinska-Kempisty, A. Poma, S. Piletsky, and N. A. Barlev: Nano Lett. **18** (2018) 4641. https://doi.org/10.1021/acs.nanolett.7b03206
34 I. Dmitriev, I. Kuryndin, N. Bobrova, and M. Smirnov: Mater. Today Commun. **4** (2015) 93. https://doi.org/10.1016/j.mtcomm.2015.06.005
35 G. C. Tong, W. K. Cornwell, and G. E. Means: Toxicol. Lett. **147** (2004) 127. https://doi.org/10.1016/j.toxlet.2003.10.021
36 M. Dockal, D. C. Carter, and F. Ruker: J. Biol. Chem. **275** (2000) 3042. https://doi.org/10.1074/jbc.275.5.3042
37 M. Punyiczki, J. A. Norman, and A. Rosenberg: Biophys. Chem. **47** (1993) 9. https://doi.org/10.1016/0301-4622(93)80028-H
38 I. G. Zigoneanu, C. E. Astete, and C. M. Sabliov: Nanotechnology **19** (2008) 105606. https://doi.org/10.1088/0957-4484/19/10/105606
39 S. Shekhar, M. Mukherjee, and A. K. Sen: Iran. Polym. J. **21** (2012) 895. https://doi.org/10.1007/s13726-012-0094-2
40 M. Koga and S. Kasayama: Endocr. J. **57** (2010) 751. https://doi.org/10.1507/endocrj.K10E-138